dimethylsilyl cation (180 kcal mol^{-1})[25] and H^+ (367.2 kcal mol^{-1})[26] yields a value of 18 kcal mol^{-1} for the heat of formation of 1-methylsilaethylene. This is in reasonable accord with Walsh's estimate of 23 ± 5 kcal mol^{-1}.[9b]

A π bond energy of 42 kcal mol^{-1} for 1-methylsilaethylene may be obtained as the difference between the heat of formation of the silaolefin and that for its corresponding biradical, Me(H)Si•–CH_2•. While the latter quantity is not known experimentally, a value of 60 kcal mol^{-1} may be estimated by combining the heats of formation of the dimethylsilane[9b] and H•[26] with its Si–H[9b] and C–H bond dissociation energies:

$$\Delta H_f(\mathrm{Me(H)Si{\bullet}{-}CH_2{\bullet}}) = D_e(\mathrm{Si{-}H}) + D_e(\mathrm{C{-}H}) + \Delta H_f(\mathrm{Me_2SiH_2}) - 2\Delta H_f(\mathrm{H{\bullet}})$$

This compares reasonably to estimates for the π bond strength in 1,1-dimethylsilaethylene.[9,11] Interestingly, the measured proton affinity of 1-methylsilaethylene is approximately 20 kcal mol^{-1} greater than that of propene, nearly identical with the suggested difference in π bond strengths between the two molecules.

Quinuclidine (ΔH = −28.1 kcal mol^{-1}) was the strongest base considered for which (silicon) dedeuteration was not observed. Triethylamine (ΔH = −28.5 kcal mol^{-1}) was the weakest base considered which did result in dedeuteration, as evidenced by the production of an ion of mass corresponding to the molecular formula $(C_2H_5)_3ND^+$. As before, we assign the mean (−28.3 kcal mol^{-1}) as the actual threshold; this leads to a heat of formation of dimethylsilylene of 46 kcal mol^{-1}. While this is in good accord with a value of 44 kcal mol^{-1} obtained by Neudorfi and Strausz from rate data on the pyrolysis of dimethylsilane, it is in poor agreement with Walsh's estimate of 26 kcal mol^{-1} for $\Delta H_f(298)$ for the species.[9b]

The present heats of formation of both 1-methylsilaethylene and dimethylsilylene depend directly on the heat of formation of their common precursor, dimethylsilyl cation. Any error in thermochemistry here leads to an equal error for the two neutrals. Note, however, that the observed 28 kcal mol^{-1} difference in the proton and deuteron abstraction thresholds yields directly, and without reference to any other thermochemical data, the difference in stabilities of 1-methylsilaethylene and dimethylsilylene; the former is the more stable. Our data disagree both with the experiments of Drahnak, Michl, and West[15] and of Conlin and Wood,[16] which suggest an opposite ordering of stabilities, and with the quantum chemical calculations of Schaefer,[18a] Köhler and Lischka,[18c] and Pople,[18d] which depict isomers of nearly equal stability.

Note also that our data provide indirect support for the notion that interconversion of 1-methylsilaethylene and dimethylsilylene proceeds only with significant barrier, as the theoretical calculations of Schaefer and his co-workers suggest.[18a,b] The fact that independent proton and deuteron thresholds are observed implies to us a significant barrier to isomerization. Previous ICR experiments with the hydrogen cyanide–hydrogen isocyanide[19d] and formaldehyde–hydroxymethylene[19e] tautomeric equilibria, both of which are known from theory to involve high interconversion barriers,[28] also revealed distinguishable thresholds. On the other hand, efforts to generate the trimethylenemethane biradical in the gas phase[29] lead instead (apparently) to methylenecyclopropane, consistent with theoretical work which shows a barrier of only a few kcal mol^{-1}.[30]

The disagreement of the present experimental thermochemical results with the high-level quantum chemical calculations of Schaefer, Köhler and Lischka and of Pople[18] is particularly disturbing. It is possible, although it does not seem likely, that our data might lend itself to alternative interpretation. Reasonable possibilities include the existence of a sizeable barrier to dedeuteration of dimethylsilyl cation, preferential formation of excited-state (triplet) as opposed to ground-state (singlet) dimethylsilylene or generation of yet another C_2H_6Si isomer. It is also conceivable that the theoretical calculations on these silicon-containing species are not as reliable in their prediction of relative thermochemical stabilities as experience, wholly with molecules containing first-row elements, suggests. Further experimental and/or theoretical work seems to be required.

Registry No. 3, 38063-40-0; **4**, 6376-86-9; $(CH_3)_2SiD_2$, 1066-41-7.

(24) (a) The original value of 202.3 kcal mol^{-1} for the proton affinity of the ammonia standard as derived from ICR spectroscopy, (J. F. Wolf, R. H. Staley, I. Koppel, M. Taagepera, R. T. McIver, Jr., J. L. Beauchamp, and R. W. Taft, *J. Am. Chem. Soc.* **99**, 5417 (1977)) has been revised upward to 205 kcal mol^{-1} due to recent work; (b) 203.6 kcal mol^{-1}, S. T. Ceyer, P. W. Tiedemann, B. H. Mahan, and Y. T. Lee, *J. Chem. Phys.*, **70**, 14 (1979); (c) 207 kcal mol^{-1}, F. A. Houle and J. L. Beauchamp, *J. Am. Chem. Soc.*, **101**, 4067 (1979); (d) 209.2 kcal mol^{-1}, R. G. McLoughlin and J. C. Traeger, *ibid.*, **101**, 5791 (1979).

(25) Averaged from the appearance potentials of dimethylsilane and trimethylsilane (H. M. Rosenstock, K. Draxl, B. W. Steiner, and J. T. Herron, *J. Phys. Chem. Ref. Data, Suppl. 1*, **6** (1977)) and their heats of formation.[9b]

(26) D. R. Stull and H. Prophet, *Natl. Stand. Ref. Data Ser. (U.S. Natl. Bur. Stand.)*, **37** (1971).

(27) P. S. Neudorfi and O. P. Strausz, *J. Phys. Chem.*, **82**, 241 (1978).

(28) See ref 19d and 19e for references to theoretical work on barrier heights.

(29) C. F. Pau, W. J. Hehre, and P. Dowd, unpublished results.

(30) W. J. Hehre, L. Salem, and M. R. Willcott, *J. Am. Chem. Soc.*, **96**, 4328 (1974).

Mechanism of Iron Dissolution and Passivation in an Aqueous Environment: Active and Transition Ranges

Alfred B. Anderson* and N. C. Debnath

Contribution from the Chemistry Department, Case Western Reserve University, Cleveland, Ohio 44106. *Received July 1, 1982*

Abstract: Structures and stabilities of FeOH, $(FeOH)^+$, $FeOH(H_2O)_5^+$, $Fe(OH)_2$, $Fe(OH)_2(H_2O)_4$, $Fe(H_2O)_6^{2+}$, and $Fe(H_2O)_6^{3+}$ are determined and analyzed using an atom superposition and electron delocalization (ASED) molecular orbital theory. The bonding of an Fe atom, FeOH, and $Fe(OH)_2$ to an Fe(100) surface is compared and contrasted. The theory supports a surface iron dissolution mechanism where, at sufficiently anodic potentials, surface FeOH species desorb as $(FeOH)^+$ and are solvated as $FeOH(H_2O)_5^+$. Evidence is presented for the precipitation of solid $Fe(OH)_2$ formed by hydrolysis of $FeOH(H_2O)_5^+$.

Introduction

A protective passive film of approximately 40 Å thickness forms on ferrous metals exposed to the atmosphere. An understanding of the passive film's mechanism of formation, structures, and failures due to active anions such as chloride has been sought for many years.[1]

0002-7863/83/1505-0018$01.50/0

Recent high-vacuum experimental[2] and quantum chemical[3] studies of reactions of water on clean and oxidized iron surfaces show dehydrogenation leading to surface OH species with small barriers of a few kcal/mol and at temperatures in the 100–200 K range. The probable significance of OH formation on clean iron surfaces in a vacuum to the phenomenon of passive film formation on similar surfaces exposed to the atmosphere may be seen using electrochemistry. Several stages go into passive film formation as an iron electrode is swept −0.5 V to +0.3 V (vs. normal hydrogen electrode). These stages are recognized if we plot current flow as a function of potential. There are five current vs. potential ranges of interest, and in weakly acidic solutions they behave as follows[4]: (i) rapidly rising current from −0.45 to −0.35 V (called the active range); (ii) relatively constant current from −0.35 to −0.25 V (called the transition range); (iii) relatively slowly rising current from −0.25 to +0.20 V (called the prepassive range); (iv) sharp drop in current from 0.20 to 0.25 V (beginning of the passive range); and (v) the current remains at a low level for about 1 V further in the anodic direction until oxygen evolution commences (called the passive range).

At very high pH the electrode surface is passivated from −0.6 to +1.4 V and there is no prepassive step.[4b] This suggests that the formation of surface hydroxyl species is an early step in passive film growth.

There appears to be no proof as yet that the electrochemically formed passive film is the same as the air-oxidized one, or that its growth mechanism is the same. The structure and exact compositions of passive films are not yet known except that they contain water or water-derived hydroxyl ligands and may have little structural long range order except when dried. However, mechanisms have been postulated to account for the steps in the electrochemical process and these mechanisms can be tested with molecular orbital theory.

It is generally agreed that at the electrode surface the initial product of the iron + water reaction is $(FeOH)_{ads}$.[1,4,5] Throughout the active transition and pre-passive ranges it is supposed[1,4] that $(FeOH)_{aq}^+$ dissolves from the surface and that in the transition range $Fe(OH)_{2,ads}$ forms and slows the dissolution of $(FeOH)_{aq}^+$ from the surface.

The purpose of this paper is to explore the formation and stabilities of species formed in the active and transition ranges. We use an atom superposition and electron delocalization (ASED) molecular orbital theory which has been found appropriate for organometallic, surface, and solid-state structure and reaction studies. Recent examples include the structure determination of an iron complex,[6] water dissociation and redox reactions on an iron surface[3a] and electrode,[3b] and the interpretation of optical spectra for ferrous and ferric oxides, and the passive film.[7] High-spin cluster models are used to approximate bulk and surface properties. The parameters used in the present work are tabulated in ref 3b.

Formation of FeOH and Dissolution of $FeOH^+$

Adsorbed FeOH forms when water contacts clean iron, and as model quantum chemical calculations have shown,[3b] as the surface potential goes anodic (modeled by shifting the Fe valence bands), the FeO bond order increases and OH gains a positive charge. On the basis of these theoretical results it was suggested in ref 3b that at a potential of 1–2 V on a relative scale deprotonation should occur because of the stability resulting from solvation of H^+. This would lead to O_2 formation. At +1 V on the scale OH has a charge of 1 on the Fe_5 cluster model and at +2 V it is 1.55. Dissolution of $(FeOH)^+$ is expected to take place at lower potentials corresponding to the pre-passive ranges, perhaps in the 0–1 V range.

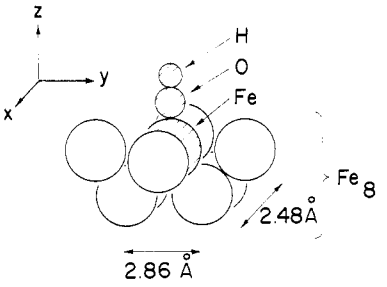

Figure 1. Coordinate system and Fe_9 cluster model of the (100) surface with adsorbed OH.

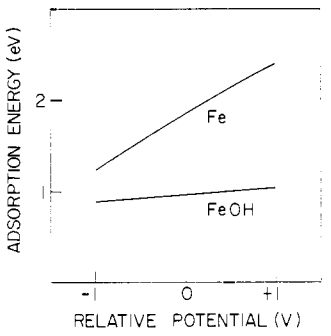

Figure 2. Relative weakening of Fe–surface (model in Figure 1) bond due to adsorption of OH.

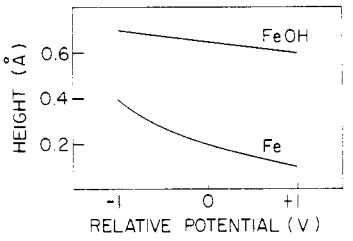

Figure 3. Relative lengthening of Fe–surface (model in Figure 1) bond due to adsorption of OH.

In the earlier study it was seen that the binding energy of OH to the surface increased with potential shifts in the anodic direction and that adsorption to onefold sites became favored (at relatively cathodic potentials bridging sites were more stable). In order to model dissolution of $(FeOH)^+$ in the anodic range, the binding energies of Fe and FeOH to a surface site in a two-layer (4 + 4) Fe_8 cluster model of the (100) surface (See Figure 1) were calculated as functions of potential. As shown in Figure 2, the binding of a centrally fully coordinated surface Fe atom is reduced when OH is coordinated to it. The figure indicates a rapid strengthening of surface Fe bonds and a slow increase in FeOH to surface bonds in the anodic direction. Corresponding contractions of surface Fe height and the FeOH height are evident in Figure 3. (The trends are what is important in our analysis; we did not optimize parameters in our semiempirical theory to produce Fe–Fe bulk bond lengths, which, though it would result in better absolute results for our surface study, would yield no additional insight.)

The predicted strengthening of the adsorption bonds on going anodic is a result of the associated stabilization of all diagonal and off-diagonal Hamiltonian energy matrix elements. Diagonal elements, H_{ii}, equal atomic orbital ionization potentials × (−1). Off-diagonal elements, H_{ij}, are equal to $1.125(H_{ii} + H_{jj})S_{ij}e^{-0.13R}$, where S_{ij} is the atomic orbital overlap integral and R is the

(1) R. P. Frankenthal and J. Kruger, Ed., "Passivity of Metals", Electrochemical Society, Princeton, 1978.
(2) (a) M. W. Roberts and P. R. Wood, *J. Electron Spectrosc. Relat. Phenom.*, **11**, 431 (1972); (b) D. J. Dwyer, G. A. Simmons, R. P. Wei, *Surf. Sci.*, **64**, 617 (1977); (c) A. G. Aklmov, *Elektrokhimya*, **15**, 1510 (1979); (d) D. J. Dwyer, S. R. Kelemen, and A. Kaldor, *J. Chem. Phys.*, **76**, 1832 (1982); (e) N. H. Turner, R. J. Colton, and J. S. Murday, "Oxidation of Iron by O_2, H_2O, and a O_2/H_2O Mixture", Naval Research Laboratory Summary Abstract, unpublished.
(3) (a) A. B. Anderson, *Surf. Sci.*, **105**, 159 (1981); (b) A. B. Anderson and N. K. Ray, *J. Phys. Chem.*, **86**, 488 (1982).
(4) (a) A. A. El Miligy, D. Geana, and W. J. Lorenz, *Electrochim. Acta*, **20**, 273 (1975); (b) N. Sato, p 29 in ref 1.
(5) T. G. Stepina and Z. A. Iofa, *Elektrokhimiya*, **16**, 888 (1980).
(6) A. B. Anderson and G. Fitzgerald, *Inorg. Chem.*, **20**, 3288 (1981).
(7) N. C. Debnath and A. B. Anderson, *J. Electrochem. Soc.*, **129**, 2169 (1982).

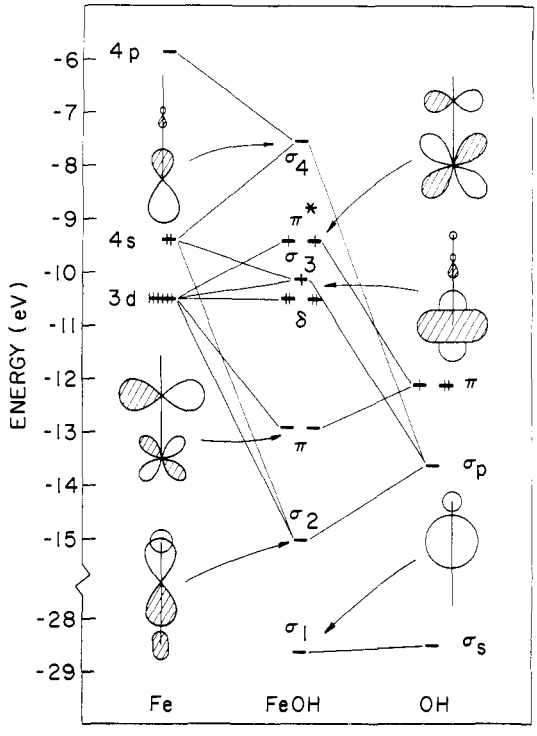

Figure 4. Bonding of Fe to OH in a linear configuration.

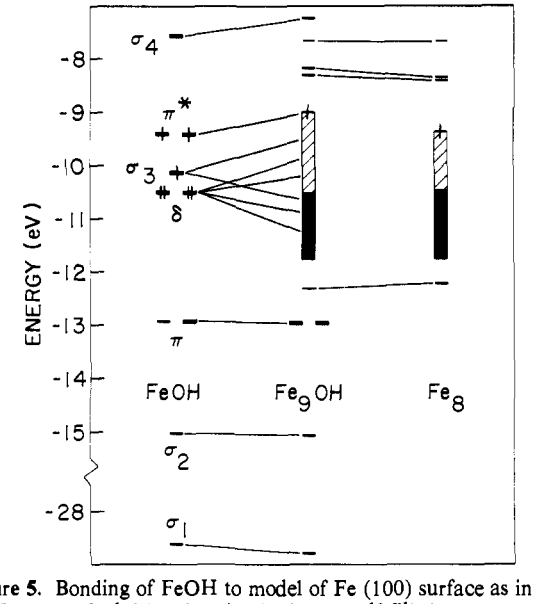

Figure 5. Bonding of FeOH to model of Fe (100) surface as in Figure 1. Cross-hatched d-band region indicates half-filled levels.

corresponding internuclear distance. The solution to this Hamiltonian gives an approximation to the bond electron delocalization energy which is added to a repulsive atom superposition energy which itself depends on atomic charge density functions. In our present model the atomic densities and atom superposition energies are not given any potential dependence. Hence changes in bond strength are due to variations in the electron bond delocalization energy. A two-state system, e.g. H_2^+, will make the desired point. The orbital energy is equal to $(H_{ii} + H_{ij})/(1 + S_{ij})$, which means there will be stronger and stronger bonding as the ionization potential, $-H_{ii}$, is increased.

The weaker bonding of FeOH to the Fe_8 surface, compared to Fe, is a consequence of shifts in atomic Fe 3d energy levels brought about by bonding to OH. These shifts are evident in the energy level diagram of Figure 4. FeOH must bond to the surface using δ nonbonding and destabilized σ_d and π_d FeOH molecular orbitals. The result is shown in Figure 5. The FeOH π^* orbitals are nonbonding to the surface and slightly destabilized. This

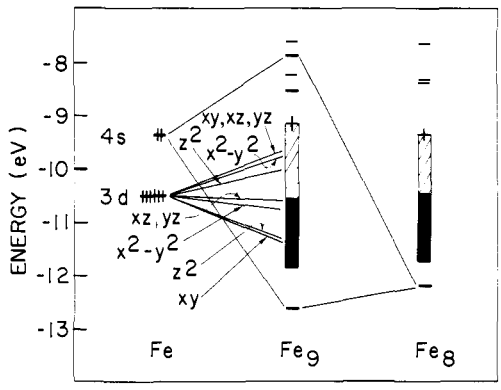

Figure 6. Bonding of top central atom in Figure 1 without OH.

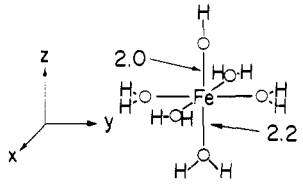

Figure 7. Octahedral geometry assumed for $FeOH(H_2O)_5^+$.

contrasts to the binding of the Fe atom to the surface (Figure 6) where the corresponding d_{xz} and d_{yz} experience stabilizing bonding interactions with the surface. A comparison of Figures 5 and 6 shows that the other three d-based orbitals in Fe and FeOH behave similarly on adsorption. In conclusion, the Fe–OH π^* bonding effectively saturates two Fe d orbitals, removing their ability to bond to the surface. This weakens the bonding and causes FeOH to establish an equilibrium height above the surface Fe atomic layer.

We note that in our model at 0 V potential the calculated Fe–OH and $(Fe–OH)^+$ bond strengths are both 2.9 eV. The values are the same because, as shown in Figure 4, to form $(Fe–OH)^+$ from FeOH an electron is removed from a nonbonding δ orbital. Experimental values[8] of 3.3 ± 0.2 eV for Fe–OH and $(Fe–OH)^+$ confirm our description of the bonding, though the accuracy of the calculated values is fortuitous. The fact that experimental values are the same means orbital relaxations and energy level shifts that go with forming $(FeOH)^+$ do not cause a qualitative departure from the nonself-consistent one-electron molecular orbital approximation used to estimate the electron delocalization energy in the ASED theory.

In our model five water molecules will bond to $(FeOH)^+$, forming octahedral $FeOH(H_2O)_5^+$ (Figure 7) with a stability gain of 2.8 eV. Subtracting the calculated desorption energy of FeOH at 0 V, the net stability given is 1.8 eV. These qualitative results say $(FeOH)_{aq}^+$ should form over a wide potential range, from active to passive.

Free energy changes, $\Delta G = \Delta H - T\Delta S$ will determine reaction outcomes. We do not have enough information to estimate the entropy changes, ΔS. Energy changes should be nearly equal to enthalpy changes, ΔH. Our estimated energy changes allow us to make suggestive energy stability arguments only and entropy contributions to ΔG could force actual equilibria in the opposite direction. Experimental values for free-energy changes of a number of reactions considered in this paper are available.[9]

X-ray diffraction studies of concentrated ferric chloride solutions produce $Fe–OH_2$ coordination bond lengths of about 2.0 Å,[10] 0.2 Å shorter than those calculated in our model. Our calculated Fe–OH distance is 2.0 Å and is probably overestimated a similar amount. Though we treated the ferrous ion in $FeOH(H_2O)_5^+$, structures for the ferric species should be similar. This is because, as shown in Figure 8, the electron comes out of a nearly nonbonding (but slightly antibonding) Fe 3d orbital. One sees in

(8) E. Murad, *J. Chem. Phys.*, **73**, 1381 (1980).
(9) T. Misawa, *Corros. Sci.* **13**, 659 (1973).
(10) M. Magini and T. Radnai, *J. Chem. Phys.*, **71**, 4255 (1979).

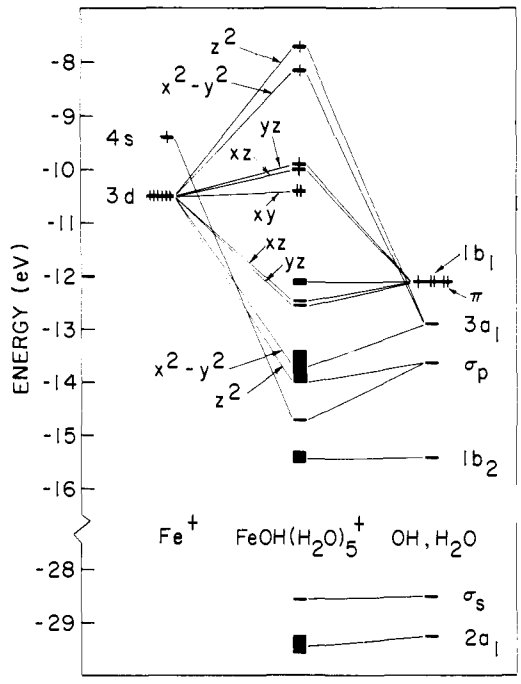

Figure 8. Bonding in $FeOH(H_2O)_5^+$.

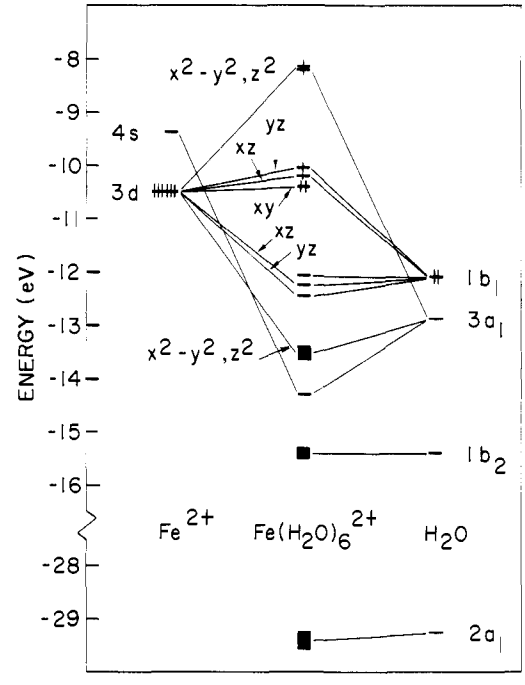

Figure 9. Bonding in $Fe(H_2O)_6^{2+}$ (structure as in Figure 7).

Figure 8 the expected splitting of the antibonding Fe-ligand d orbital levels resulting from imperfect octahedral coordination. A study of $Fe(H_2O)_6^{2+}$ produces a similar energy level structure, shown in Figure 9. The t_{2g}- and e_g- derived energy levels are split because of the geometry—the structure is as in Figure 7 with OH replaced by H_2O. Our calculated Fe–O bond length is 2.17 Å. For $Fe(H_2O)_6^{3+}$ this shrinks only 0.01 to 2.16 Å because the oxidized electron comes from a weakly antibonding orbital. This contrasts with ferrous and ferric Fe–O bond length variations of several tenths of an angstrom in the bulk oxides, as discussed in ref 7.

It is interesting that our calculations produce water rotation barriers of under 1 kcal/mol for all water coordinated species treated in this paper. This is because the H_2O $3a_1$ lone-pair orbital mixes strongly with Fe orbitals and is invariant to rotation. The $1b_2$ lone-pair orbital, though sensitive to rotational orientation, mixes weakly as in Figures 8 and 9.

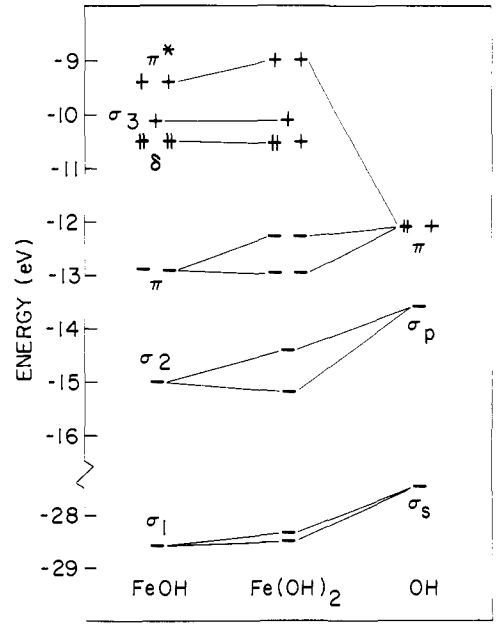

Figure 10. Bonding of OH to FeOH to form linear $Fe(OH)_2$.

Formation and Precipitation of $Fe(OH)_2$

The free-energy change for the reaction

$$(FeOH)_{aq}^+ + H_{aq}^+ \rightarrow Fe_{aq}^{2+} + H_2O \qquad (1)$$

is −9.2 kcal/mol +1.36 pH,[9] so that in acidic solutions Fe_{aq}^{2+} formation will be favored. Other reactions may lead directly to passive film formation. For example

$$(FeOH)_{aq}^+ + H_2O \rightarrow Fe(OH)_2 + H_{aq}^+ \qquad (2)$$

with a free energy change of 6.3 kcal/mol −1.36 pH[9] will be favored in basic solutions.

Assuming that $Fe(OH)_2$ formation is a step passed through in the formation of the passive films, it forms immediately at pH 11.5 and greater from −0.6 to +1.4 V.[4b] At lower pH values the current peak corresponding to active, transition, and pre-passive stages is measured in the −0.6 to +0.4 V range, while at pH 11.5 the iron surface is passivated until the onset of oxidation at 1.4 V.[4b] Consequently, in addition to (2), a second mode of $Fe(OH)_2$ formation is likely

$$Fe + H_2O \rightarrow FeOH_{ads} + H$$

$$FeOH_{(ads)} + H_2O \rightarrow Fe(OH)_{2(ads)} + H \qquad (3)$$

In this section we present our analyses of (2) and (3).

Our calculations produce linear $Fe(OH)_2$ with Fe–OH bond lengths of 1.73 Å, 0.10 longer than for FeOH. The ligand orbital energy levels split into binding and antibonding sets (Figure 10). Antibonding destabilizations cause the π^* levels to shift up but the δ and σ_3 levels are unmoved. We assign four unpaired electrons. Our calculated binding energy for $Fe + 2OH \rightarrow Fe(OH)_2$ is 4.9 eV. Since the heat of vaporization of Fe metal is 3.7 eV (our results in Figure 2 underestimate this), the energetics favor formation of ferrous hydroxide, and at high pH this appears to form directly. Our calculations produce a weak binding interaction of $Fe(OH)_2$ with the hole surface site in the Fe_8 cluster (0.9 eV at a height of 2.15 Å parallel to the surface). A similar weak interaction energy is obtained between two parallel $Fe(OH)_2$ molecules (0.8 eV when separated by 2.7 Å). Such predicted weakness suggest that, though $Fe(OH)_2$ molecules are stable, structural rearrangements should occur in the solid $Fe(OH)_2$. Treatment of the structure of solid $Fe(OH)_2$ is outside the scope of this work.

A second mode of $Fe(OH)_2$ formation involves the reaction given in (2). In our model we express this as

$$Fe(OH)(H_2O)_5^+ \rightarrow Fe(OH)_2(H_2O)_4 + H_{aq}^+ \qquad (4)$$

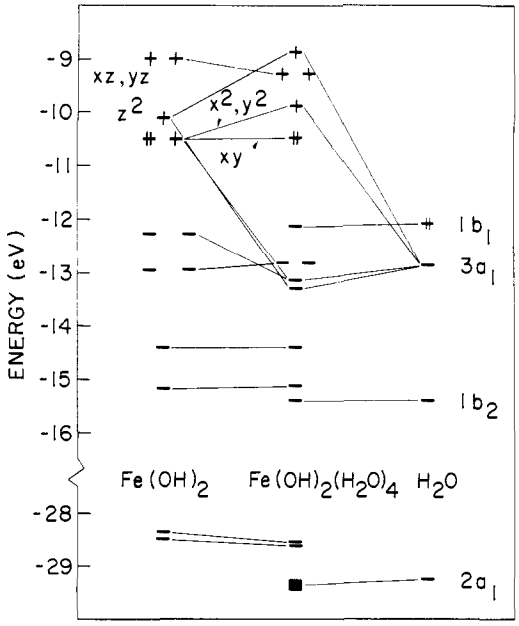

Figure 11. Bonding of water to $Fe(OH)_2$ to form $Fe(OH)_2(H_2O)_4$.

Our calculated destabilization energy is 4.7 eV. The proton solvation energy has been calculated to be ~5 eV,[3b] which will counter this energy increase. For the stripping of the four water molecules in $Fe(OH)_2(H_2O)_4$ we calculate an energy input of 1.4 eV, but cohesion of two $Fe(OH)_2$ molecules from above is 0.8 eV. Thus the net calculated energy for the reaction 2 is +0.3 eV. The cohesive energy of bulk $Fe(OH)_2$ will overcome this small barrier, and though the entropy decrease will favor maintaining the reactants in (4), at high pH or sufficiently anodic potentials $Fe(OH)_2$ forms.

Our total calculated ligand binding energies in $FeOH(H_2O)_5^+$ and $Fe(OH)_2(H_2O)_4$ are 6.1 and 6.3 eV, respectively. The $Fe(OH)_2$ ligand bonds are accounting for 78% of the stability in $Fe(OH)_2(H_2O)_4$, with the four water molecules weakly coordinated, with an average energy of 0.4 eV. In $Fe(OH)_2(H_2O)_n$, where $n = 3$, 2, and 1, the average H_2O coordination energies are 0.18, 0.22, and 0.56 eV, respectively. Consequently, $Fe(OH)_2(H_2O)_4$, once it loses the first H_2O ligand, will lose the others readily and precipitate $Fe(OH)_2$. The weakness of the coordination of 4 H_2O ligands to $Fe(OH)_2$ has associated with it the absence of orbital energy level stabilizations indicated in Figure 11. The two axial hydroxyl ligands have tied up and "saturated" the Fe $d_{x^2-y^2}$ and d_{z^2} orbitals so that there is a weaker interaction with equatorial H_2O ligands: Compare Figures 9 and 11.

Concluding Comments

We have determined a clear-cut mechanism for anodic iron dissolution to form $(FeOH)_{aq}^+$: surface OH weaken Fe–surface bonds and $FeOH^+$ forms and leaves the surface, becoming rapidly solvated, forming $FeOH(H_2O)_5^+$.

$(FeOH)_{aq}^+$ will hydrolyze, forming $Fe(OH)_2(H_2O)_4$ which is weakly stable and will precipitate as solid $Fe(OH)_2$. This is probably a step in anodic passive film formation at low pH. At high pH the dissolution step does not seem to occur,[4b] and the mechanism may involve surface reactions.

Thermodynamics must ultimately be taken into account in any complete description of iron dissolution and passivation in an aqueous environment. Entropy changes can dominate reactions. Detailed considerations of thermodynamics are beyond the scope of our quantum chemical study. However, the structural, energetic, and mechanistic hypotheses in our work corroborate a number of hypotheses in the literature.

Acknowledgment. We thank the Office of Naval Research for supporting our work through a Select Research Opportunities Grant. We express our appreciation to members of the Case Center for Electrochemical Sciences for their congenial interest and advice.

Phosphorus NMR Study of Solid Amorphous Calcium Phosphate

James Tropp,[†] Norman C. Blumenthal,[‡] and John S. Waugh*[†]

Contribution from the Department of Chemistry, Massachusetts Institute of Technology, Cambridge, Massachusetts 02139, and The Hospital for Special Surgery, Cornell University Medical College, New York, New York 10021. *Received May 18, 1982*

Abstract: We have characterized solid synthetic amorphous calcium phosphate (ACP) by ^{31}P NMR, using magic angle spinning, proton enhancement via cross polarization, and variable temperature. With no cross polarization, the spinning sidebands of ACP are stronger than those of unprotonated phosphate in hydroxylapatite, but weaker than those of dibasic calcium phosphates. Cross polarization over a wide range of mixing times causes no change in the appearance of ACP spectra from 25 to −120 °C. In contrast, mixtures of hydroxylapatite with dibasic calcium phosphates, which, without cross polarization mimic the appearance of ACP spectra, show large differential enhancements of sideband intensities when cross polarized. Octacalcium phosphate behaves similarly to the mixtures. Vacuum drying of ACP at 450 °C removes tightly bound water. The sidebands of dried ACP are undiminished, but no cross polarization signal can be obtained. Similar drying of hydroxylapatite affects neither the sideband intensities nor the cross polarization. We conclude that the strength of ACP sidebands is due to a characteristic structural distortion of unprotonated phosphate and *not* to a mixture of protonated and unprotonated phosphates. Structural models of ACP and the implications for ^{31}P NMR studies of bone mineral are briefly discussed.

Introduction

It has long been known that formation of hydroxylapatite (HA) in vitro can occur via an amorphous precursor substance, commonly referred to as amorphous calcium phosphate (ACP).[1] When calcium phosphate is precipitated from sufficiently concentrated aqueous solution at or above neutral pH, the initial product is amorphous, as judged by X-ray diffraction, electron microscopy, and infrared spectroscopy.[2] This amorphous pre-

[†] Massachusetts Institute of Technology.
[‡] Cornell University Medical College.

(1) Eanes, E. D.; Gillessen, I. H.; Posner, A. S. *Nature (London)* **1965**, *208*, 365-367.

0002-7863/83/1505-0022$01.50/0